

Aberrant Brain Connectivity in Schizophrenia Detected via a Novel Gaussian Graphical Model

Aiying Zhang¹

Jian Fang¹

Faming Liang²

Vince D. Calhoun³

Yu-Ping Wang¹

Abstract—Schizophrenia (SZ) is a chronic and severe mental disorder that affects how a person thinks, feels, and behaves. It has been proposed that this disorder is related to disrupted brain connectivity. With the development of functional magnetic resonance imaging (fMRI), further exploration of brain connectivity was made possible and this hypothesis has been verified. Region-based networks are commonly used for mapping brain connectivity. However, they fail to illustrate the connectivity within regions of interest (ROIs) and lose precise location information. Voxel-based networks provide higher precision, but are difficult to construct and interpret due to the high dimensionality of the data. In this paper, we adopt a novel high-dimensional Gaussian Graphical Model (GGM) – ψ -learning method, which can help ease computational burden and provide more accurate inference for underlying networks. The fMRI data we used were collected by the Mind Clinical Imaging Consortium (MCIC) using an auditory task in which there are 92 SZ patients and 116 healthy controls. We compared the networks at three different scales by using global measurements, community structure, and edge-wise comparisons within the networks. Results reveal, at the highest resolution, sets of distinct aberrant patterns for the SZ patients and provides more precise local structures within ROIs for further investigation.

Index Terms—Schizophrenia (SZ), Brain connectivity, Gaussian Graphical Models (GGMs), Network comparison

I. INTRODUCTION

Schizophrenia (SZ) is a chronic and severe mental disorder that is characterized by hallucinations, derealization, delusions, loss of initiative, and cognitive dysfunction. The notion that SZ may be related to disrupted brain connectivity dates back to the 19th and 20th centuries. Pioneers like Theodor Meynert (1833–1892) and Carl Wernicke (1848–1905) first proposed that psychotic disorders might arise from abnormal connectivity of axons between different regions in the brain [1]. This hypothesis has recently been revived and generalized due to a wealth of functional magnetic resonance imaging (fMRI) data which suggest a connection between SZ and abnormal neuron networks.

By incorporating graph theory into connectivity analysis, we can gain new understanding of the characteristics of the human brain, from microscale connectivity between single neurons to macroscale connectivity between regions of interests (ROIs) or voxels in brain images. The brain can be described as a graph where nodes represent neurons or brain regions, and are linked

by edges, their interconnecting synapses or axons. A popular method to study association networks is the Gaussian Graphical Model (GGM). The key idea of a GGM is to use the partial correlation coefficient to remove confounding effects of the correlations. For brain network construction the variable size is always larger than the sample size which leads to the necessity of using high-dimensional GGMs. Various solutions have been proposed in the literature, such as nodewise regression [2] and graphical Lasso (gLasso) [3], [4]. In this paper, we adopt the ψ -learning method proposed by Liang et al. [5]. This method defines an equivalent partial correlation – ψ -correlation that keeps the properties of partial correlation without losing the inference accuracy. It is both computationally efficient for high dimensional problems and flexible for network comparison. We will discuss this method more in Section II.

Generally, one can construct brain functional networks at different scales. A common approach is to construct a region-based network with nodes corresponding to anatomically defined ROIs [6], [7]. In this way, one largely reduces the high dimensionality resulting in a lower requirement for sample size and computational efficiency. In addition, it can be easier to interpret the biological meaning of the connectivity. Another way to construct these networks is by using a voxel-based network, treating each voxel as a network node [8], [9]. Despite of intensive computational demands, there are distinct benefits of modeling the brain network at the highest resolution. According to Hayasaka and Laurienti [10], voxel-based networks are more robust against network fragmentation compared to region-based networks. Moreover, voxel-based network analyses are able to examine the inner connectivity of ROIs and thus localize hub organizations within particular anatomical areas. However, it is still a challenge to study voxel-based brain networks due to the associated computational burdens and interpretation difficulties. Some in-between approaches have been developed, such as using independent component analysis (ICA) time courses as nodes [11], [12]. In this paper, we directly target the voxel level and adopt the ψ -learning method to solve the computational problem. Compared to existing GGM algorithms, the ψ -learning algorithm is favorable with a computational complexity of nearly $O(p^2)$, whereas others are usually $O(p^3)$ or higher [5].

We compared the difference of the constructed networks in the case and control group from three aspects. First, we examined the global measurements of the networks [13] including network centrality, segregation, and integration. The centrality measurements were used to detect central brain regions, called hubs, that interact with many other regions in the global networks. Measures of segregation primarily

¹ Department of Biomedical Engineering, Tulane University, New Orleans, LA 70118, USA

² Department of Statistics, Purdue University, West Lafayette, IN 47907, USA

³The Mind Research Network, University of New Mexico, NM 87131, USA

quantify the presence of densely connected groups, known as clusters or modules. Second, we further extracted the modular information [14] and compare the modularity similarity between the case and control groups. Third, we explored the aberrant connectivity patterns by a pairwise comparison and identified the significant central aberrant hubs. As a result of all these measurements, we discovered significantly reduced connectivity, altered topology, and asymmetric patterns of the network for SZ. As described below, such voxel-level analysis allowed us to uncover novel fine-scale functional sub-patterns in brains for SZ.

The remainder of this paper is organized as follows. In Section II, we introduce the methodologies used throughout the study including ψ -learning and our network measurement method. Analysis results are shown in Section III including evaluation, measurement, and comparison. Some discussions and concluding remarks are made in the last section.

II. METHODS

In this section, we present our analysis approach (see Figure 1) including network construction, global measurements, and pairwise comparison. We also provide a detailed discussion of the methods and algorithms we propose.

A. ψ -learning method

The ψ -learning method is one kind of GGM which can deal with high-dimension but small sample size data. As usual, Pearson correlation coefficients are used in network analysis. However, all the variables in the network system are directly or indirectly, more or less correlated. It is difficult to distinguish direct connections through a dense network and thus GGMs are commonly applied. The main idea is to use the partial correlation coefficient as a measure of dependency for any two variables. A zero partial correlation indicates conditional independence, i.e., the two variables are not directly correlated. More precisely, let $X = (X_1, \dots, X_p)$ denote a p -dimensional random vector following a multivariate Gaussian distribution $N(\mu, \Sigma)$, where μ and Σ denote the unknown mean and covariance matrix, respectively. With the efforts of mathematicians and statisticians [15], [16], it was proven that the partial correlation between X_i and X_j can be expressed as

$$\rho_{ij|V \setminus ij} = -\frac{\Omega_{i,j}}{\sqrt{\Omega_{i,i}\Omega_{j,j}}}, i, j = 1, \dots, p \quad (1)$$

where Ω is the precision matrix (i.e., inverse of the covariance matrix Σ), $\Omega_{i,j}$ denotes the (i,j) th entry of Ω and $V = \{1, 2, \dots, p\}$ denotes the set of indices of variables.

Thus, the constructions of GGMs are equivalent to the estimation of the precision matrices. In practice, we often meet the case that the sample size n is smaller than the variable size p . Then the covariance matrix Σ is singular and hence the precision matrix Ω cannot be directly estimated. Liang et al. [5] proposed a novel high-dimensional GGM – the ψ -learning method, which could solve the concerns with higher computational efficiency while providing precise inference. They defined an equivalent measure of partial correlation, called

the ψ -correlation, which avoids inverting high-dimensional matrices. The definition of the ψ -correlation between X_i and X_j is given by

$$\psi_{ij} = \rho_{ij|S_{ij}} \quad (2)$$

where S_{ij} is a reduced neighboring set of X_i or X_j , and it can be obtained through a correlation screening procedure. In this way, we invert a smaller dimensional matrix for each pair. Details are discussed in the Section II-B. Liang et al. has proven that the ψ -partial correlation coefficient is equivalent to the true partial correlation coefficient in the sense that

$$\psi_{ij} = 0 \iff \rho_{ij|V \setminus ij} = 0 \quad (3)$$

This method has been proven to be consistent under mild conditions, i.e. the network will converge to the true one as the sample size goes to infinity. The ψ -correlation keeps similar properties to the partial correlation which makes it very easy to do network comparison for the case-control study.

B. Algorithm Structure

The algorithm structure of the ψ -learning method consists of three main parts: correlation screening, ψ -calculation, and ψ -screening. The screening procedures are designed to control the density of the constructed network, which is achieved through multiple hypothesis tests. To do this, we first convert the correlation coefficients and the ψ -correlation coefficients to z -scores and ψ -scores via Fisher's transformation, respectively.

$$z_{ij} = \frac{\sqrt{n-3}}{2} \log \left[\frac{1 + \hat{r}_{ij}}{1 - \hat{r}_{ij}} \right] \quad (4)$$

$$\psi_{z_{ij}} = \frac{\sqrt{n - |S_{ij}| - 3}}{2} \log \left[\frac{1 + \hat{\psi}_{ij}}{1 - \hat{\psi}_{ij}} \right] \quad (5)$$

where n is the sample size, p is the number of variables and \hat{r}_{ij} , $\hat{\psi}_{ij}$ are the empirical correlation coefficient and empirical ψ -correlation coefficient of X_i and X_j , $i, j = 1, \dots, p$, respectively. Under the null hypotheses ($H_0^z : r_{ij} = 0$, $H_0^\psi : \psi_{z_{ij}} = 0$), the z -scores and ψ -scores follow a standard normal distribution $N(0, 1)$.

The essence of the ψ -learning method is to identify the reduced conditional set S_{ij} . After correlation screening, we detect the pairs of variables whose empirical correlation coefficient is significantly different from zero and form a sparser correlation matrix. According to previous work [5], we set a global size bound of the neighborhood size $\gamma = n/\log(n)$. If the neighborhood size of variable X_i exceeds γ , we remove the variables having a lower correlation (in absolute value). For each pair of variables X_i and X_j , we simply choose the neighborhood set that has less elements as S_{ij} . This results in a reduced correlation network. Based on the definition given in equation (2), we calculate $\psi_{ij} = \rho_{ij|S_{ij}}$ by inverting the subsample covariance matrix indexed by the variables in $S_{ij} \cup \{i, j\}$. Finally, we implement a screening process to make the network sparse.

The multiple hypothesis tests used in this paper are implemented via a generalized empirical Bayesian method proposed by Liang and Zhang [17]. As one of the FDR control methods,

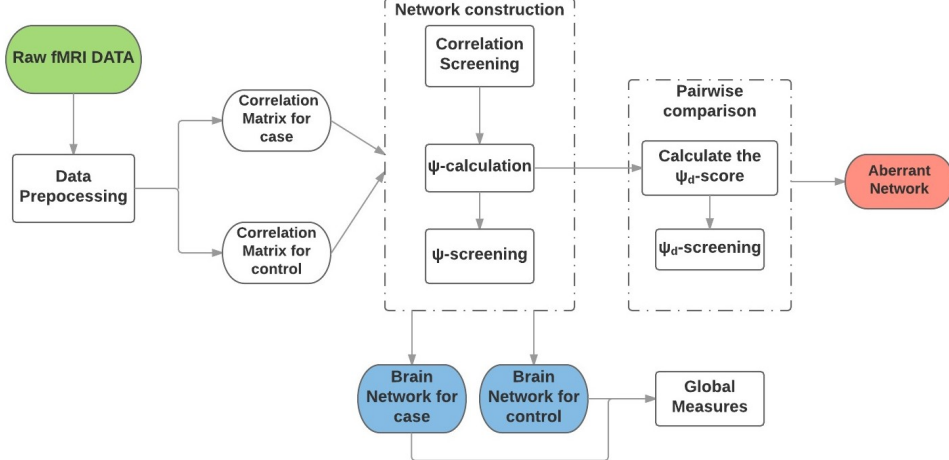


Figure 1: The flowchart for the study procedure

its main advantage is that this method allows for the general dependence between test statistics.

Therefore, the algorithm of the ψ -learning method can be summarized as follows:

1) Correlation Screening

- Calculate the empirical covariance matrix $\hat{\Sigma}$ to get the correlation coefficient \hat{r}_{ij} for each pair of nodes i, j , $i, j = 1, \dots, p$.
- Conduct a multiple hypothesis test at significance level α_1 and get the reduced correlation network.

2) ψ -calculation

Calculate $\psi_{ij} = \rho_{ij|S_{ij}}$ by inverting the subsample covariance matrix indexed by the variables in $S_{ij} \cup \{i, j\}$.

3) ψ -screening

Conduct a multiple hypothesis test on the ψ -score at significance level α_2 to obtain the adjacency matrix.

The R package *equSA* for ψ -learning is now publicly available at <https://cran.r-project.org/web/packages/equSA/index.html>.

C. Network Comparison

We aim to find the difference in brain connectivity between the SZ patients (case group) and healthy individuals (control group). We apply the ψ -learning method to both groups. Let $\psi_{z_{ij}}^{(1)}$ and $\psi_{z_{ij}}^{(2)}$ denote the statistics obtained from condition 1 (case group) and condition 2 (control group), respectively. Then the test statistics of their difference is

$$\psi_{d_{ij}} = (\psi_{z_{ij}}^{(1)} - \psi_{z_{ij}}^{(2)})/\sqrt{2} \quad (6)$$

where $\psi_{d_{ij}}$ follows the distribution of $N(0, 1)$. Then the problem of network comparison is transferred to a multiple testing problem: simultaneously testing, $H_0^{(ij)} : e_{ij}^{(1)} = e_{ij}^{(2)} \leftrightarrow H_1^{(ij)} : e_{ij}^{(1)} \neq e_{ij}^{(2)}$ for all $1 \leq i < j \leq p$, where $e_{ij}^{(k)}$ is the indicator of the edge between node i and node j for the

network constructed under condition k , $k = 1, 2$. In our case, $k = 1$ stands for the case group and $k = 2$ stands for the control group. We use the same test procedure mentioned in Section II-B and set the significance level at α_3 .

In summary, the algorithm is as follows:

- Perform Steps 1 and 2 of ψ -learning algorithm independently for each source of data
- Calculate the difference of ψ -score – ψ_d -score.
- Conduct a multiple hypothesis test to identify the pairs of nodes for which $\psi_{d_{ij}}$ is differentially distributed from the standard normal $N(0, 1)$.

D. Network Measurements and Evaluations

It is difficult to interpret a large-scale network or network difference comprehensively only from the raw network, especially at the voxel level. Complex brain networks can be characterized by several aspects of global network measurements which can also keep neurobiological meaning. In this paper, we consider the measures of functional segregation, functional integration, and centrality discussed by Rubinov and Sporns [13].

Let P denote the set of nodes in the network and p the number of nodes (corresponding to the number of variables). $E_{p \times p}$ denotes the adjacency matrix of a network and e_{ij} is the ij -th entry of E which represents the connection status of nodes i and j (i.e., variables X_i and X_j): $e_{ij} = 0$ indicates there is no edge between nodes i and j ; otherwise there is an edge between nodes i and j . Table I gives a list of network measurements including basic concepts (*degree*, *number of triangles* and *shortest path length*), functional segregation (*clustering coefficient*, *transitivity* and *local efficiency*), functional integration (*characteristic path length*, *global efficiency*), and centrality (*degree*, *betweenness centrality*). Moreover, we also detect network modularity using Newman's spectral community detection [14].

Table I: A List of Network Measures and Evaluations

Measure/Evaluation	Definition
Degree	$k_i = \sum_{j \in P} e_{ij}$
Number of Triangles	$t_i = \frac{1}{2} \sum_{j,h \in P} e_{ij} e_{jh} e_{ih}$
Shortest Path Length ¹	$d_{ij} = \sum_{e_{uv} \in g_{i \leftrightarrow j}} e_{uv}$
Characteristic Path Length	$L = \frac{1}{p} \sum_{i \in P} \frac{\sum_{j \in P, j \neq i} d_{ij}}{p-1}$
Clustering Coefficient	$C_i = \frac{1}{p} \sum_{i \in P} \frac{t_i}{k_i(k_i-1)}$ (of node) $C = \frac{1}{p} \sum_{i \in P} C_i$ (of network)
Transitivity	$T = \frac{\sum_{i \in P} 2t_i}{\sum_{i \in P} k_i(k_i-1)}$
Global Efficiency	$E_{glo} = \frac{1}{p} \sum_{i \in P} E_i = \frac{1}{p} \sum_{i \in P} \frac{\sum_{j \in P, j \neq i} d_{ij}^{-1}}{p-1}$
Local Efficiency ²	$E_{loc} = \frac{1}{p} \sum_{i \in P} E_{loc,i} = \frac{1}{p} \sum_{i \in P} \frac{\sum_{j,h \in P, j, h \neq i} e_{ij} e_{ih} [d_{jh}(i)]^{-1}}{k_i(k_i-1)}$
Betweenness Centrality ³	$b_i = \frac{1}{(p-1)(p-2)} \sum_{h,j \in P, h \neq j, h \neq i, i \neq j} \frac{\rho_{hj}^{(i)}}{\rho_{hj}}$
Degree Distribution	Power Law: $P(X = x) \propto x^{-\nu}$, for some $\nu > 0$
Small worldness ⁴	$S = \frac{C/C_{rand}}{L/L_{rand}}$

¹ $g_{i \leftrightarrow j}$ is the shortest path (geodesic) between i and j .

² $d_{jh}(i)$ is the length of the shortest path between j and h that contains only neighbors of i .

³ ρ_{hj} is the number of shortest paths between h and j , and $\rho_{hj}^{(i)}$ is the number of shortest paths between h and j that pass through i .

⁴ C_{rand} and L_{rand} represent the clustering coefficient and characteristic path length of a random network respectively.

Two evaluation methods are considered to assess the quality of the constructed networks. One way is to examine the degree distribution. A lot of biological networks have been observed to be scale-free [18], whose degree distributions follow a power law (defined in Table I). We use this property as one of the evaluations for the constructed networks. A preliminary visual test of the power law is to fit the log-cCDF $\log P(X > k)$ versus the log-degree $\log(k)$ plot [19]. A scale-free network should have a linear, decreasing pattern. In addition, many studies have found that brain connectivity tends to be exhibited as a small world, as most nodes are not neighbors of one another, but seem to be connected by a short path through the network [6], [9]. Humphries and Gurney [20] proposed a measure of small-worldness S that compares the constructed network to a random network with the same number of nodes and edges. A small-world network often has $S \gg 1$.

The open source Matlab brain connectivity toolbox (BCT) is freely available at www.brain-connectivity-toolbox.net, and provides the functions for the network measures we discuss above. A function of generating random networks is also included.

III. RESULTS

A. Data Pre-processing

We applied the method to fMRI data collected by The Mind Clinical Imaging Consortium (MCIC). The data were from 208 subjects, among them 92 SZ patients (age: 34 ± 11 , 22 females) and 116 healthy controls (age: 32 ± 11 , 44 females). They were collected during a sensory motor task, a block design motor response to auditory stimulation. We follow the same pre-processing procedures as outlined in Lin et al. [21]. The images were acquired on a Siemens3T Trio Scanner and 1.5 T Sonata with echo-planar imaging (EPI) sequences taking parameters (TR = 2000 ms, TE = 30 ms

(3.0T)/40 ms (1.5T), field of view = 22 cm, slice thickness = 4 mm, 1 mm skip, 27 slices, acquisition matrix = 64×64 , flip angle = 90°). Data were pre-processed with SPM5 and were realigned, spatially normalized and resliced to $3 \times 3 \times 3$ mm, smoothed with a $10 \times 10 \times 10$ mm³ Gaussian kernel, and analyzed by multiple regression considering the stimulus and their temporal derivatives plus an intercept term as regressors. Finally the stimulus-on versus stimulus-off contrast images were extracted with $53 \times 63 \times 46$ voxels and all the voxels with missing measurements were excluded. In order to filter irrelevant information, we further implemented a multiple t-test between case and control groups at the voxel level. Finally, 116 ROIs were extracted based on the AAL brain atlas and $p = 9816$ voxels were left for analysis.

B. Parameter Selection and Network Evaluation

In our study, we have $n_1 = 92$ in the case group and $n_2 = 116$ in the control group. The maximum neighborhood size is set uniformly with $\gamma = \max\{\gamma_1, \gamma_2\} = \max\{n_1/\log(n_1), n_2/\log(n_2)\} = 25$. The correlation screening threshold α_1 really decides the neighborhood for each node and hence is the key of the method. We set $\alpha_1 = 0.1$ through the recommendation of Liang [5] to include as much information as possible. The screening effect is shown in Figure 2. Finally, the density of the constructed network is controlled by the ψ -screening threshold α_2 , set at 0.01.

We identified 7353 and 57388 edges with $p = 9816$ for the case and control groups, respectively. Figure 3 shows the histograms of the degrees for both groups. For small-worldness coefficients, we received $S_1 = 568.3840$ for the case group and $S_2 = 440.2775$ for the control group. We plotted the log-cCDF versus the log-degree for the constructed networks to examine the power law distribution (see Figure 3 (c),(d)). The more that the pattern is close to a linear, decreasing line, the

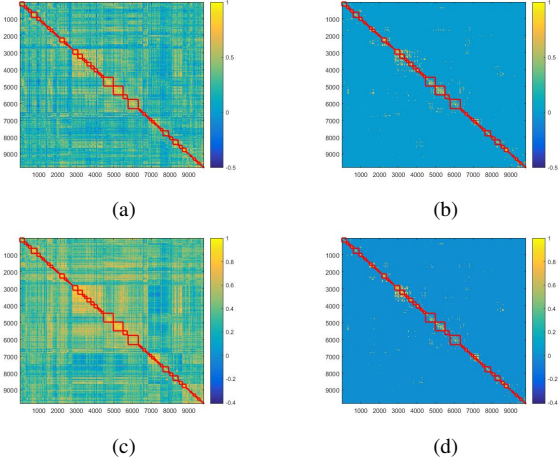


Figure 2: The visualizations of correlation matrices before (a,c) and after (b,d) correlation screening with the significance level $\alpha_1 = 0.1$. Figure (a),(b) describe the SZ patients and (c),(d) describe healthy controls

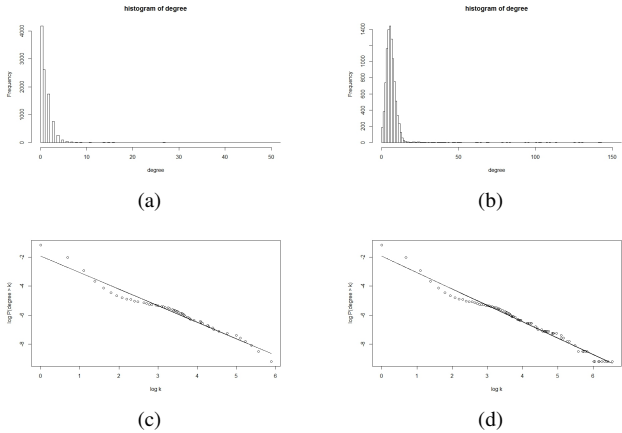


Figure 3: The histograms of the degrees of the networks for case (a) and control (b). (c),(d) show the corresponding log-log plots of the degree distributions of the networks. The curves are fitted by the linear regression function in R.

closer the network is to being scale-free. As we can see, both of the networks fit to scale-free model well.

C. Global Measures Comparison

We summarized the networks in three aspects: centrality, segregation, and integration. As we can see in Table II, the mean clustering coefficient of the case group is far larger than that of the control group, which shows, on average, it is more clustered around individual nodes in the case group. On the other hand, the transitivity, a measure of the density of triangles in a network, of the case group is bigger than that of the control group; it suggests that although there are fewer edges in the SZ network, it tends to have more transitive triples. Both the global efficiency and characteristic path length of the case group are smaller than those of the control group. This may suggest that the functional integration of the SZ brain is not as developed as healthy brains. This means the

SZ patients may not be able to rapidly combine specialized information from distributed brain regions compared to healthy people.

Table II: Basic measures for the case and control groups

Measures	Case group	Control group
Mean clustering coefficient	0.0800	0.4886
transitivity	0.0073	0.0029
Global efficiency	0.0374	0.4568
Characteristic path length	0.00015	0.0012

Prior analysis has shown that SZ patients have reduced high degree hub organizations as well as altered topology relative to healthy controls [1]. In graph theory, hubs are the vertices with high numbers of edges, i.e., degrees, which is an important measure for the centrality. At the ROI level, we first summed the voxel-voxel edges within and between ROIs to get an ROI adjacency matrix, the value of which represents the strength of the connectivity. We found that normally the connectivity among different brain regions always goes through inferior temporal gyrus (T3), cingulate gyrus, anterior part (CIA), precentral gyrus (FA) or left precuneus (PQG). Furthermore, these hub regions also have strong connectivity between each other, which form a so-called "rich club," characterized by a tendency for high-degree nodes to be more densely connected among themselves than nodes of a lower degree. On the other hand, for people who have SZ, although having significantly reduced activities, their connectivity is centered around inferior temporal gyrus (T3), caudate nucleus (NCD), left middle frontal gyrus (F2G), left inferior frontal gyrus, orbital (F3OG), left cerebellum crus 1 (CERCRU1G) and left precuneus (PQG). However, the pattern of rich club organization was destroyed (see Figure 4). The visualization of brain connectivity is done through the *BrainNet Viewer* toolbox (www.nitrc.org/projects/bnv/) [22].

One advantage of using the voxel-voxel network is that it can provide more precise information within a brain region and is thus more sensitive to topology change. We chose some significant ROIs for both groups with the criteria that the total number of connections of the specific ROI is over the threshold of mean connectivity + 3 standard deviation(sd). As shown in Figure 5, we found three patterns of hub alterations. The first pattern (Fig 5 (I)) mainly happens in FA, CIA, PQG and T3G that has a large portion of reduced edges at the hub points. The second pattern (Fig 5 (II)) suggests that there is not only overall reduced connectivity, but also a slightly change of hub points in F1D and T3D. The last pattern (Fig 5 (III)) shows that these ROIs (F2G,F3OG,NCD,CERCRU1G) are relatively active in the SZ patient's brain connectivity. Moreover, significant new hub points form in these areas. Table III gives the exact MNI space coordinates of the hub points identified in Figure 5 for both the cases and controls.

D. Community Structure

To further explore the rich club organizations, we divided the whole brain network into several sub-modules. We did this division at the voxel level which may result in some overlaps of ROIs in different modules. It makes sense that different

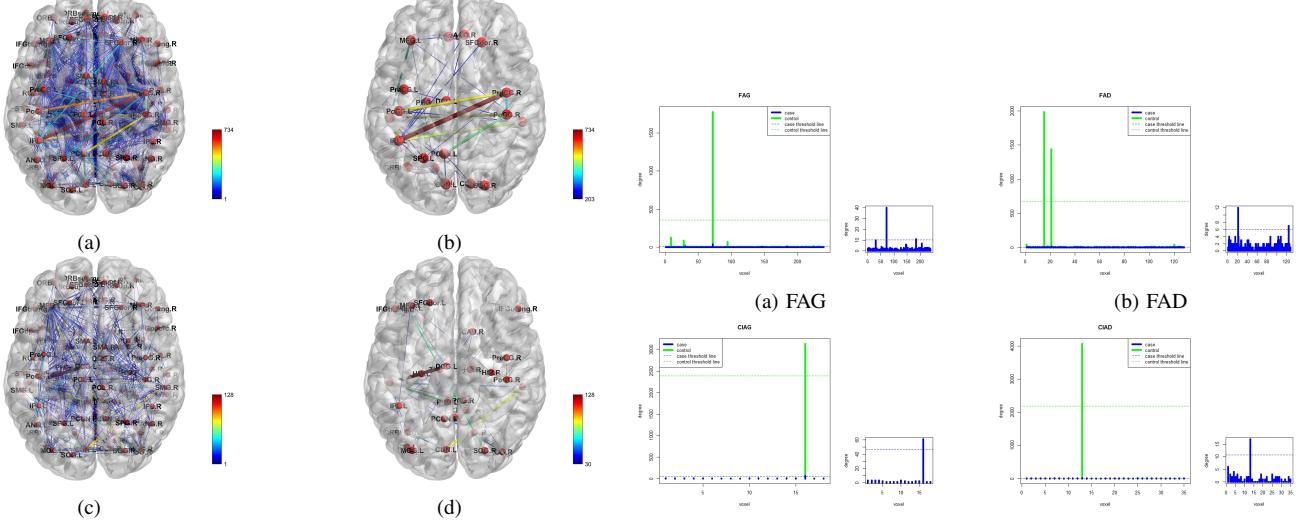


Figure 4: Axial view of the brain connectivity's on ROI level. Left column shows the full connectivity for healthy people (a) and SZ patients (c). The right column shows filtered edges with sparsity = 0.005 for healthy individuals (b) and SZ patients (d). The node size represents the amount the inter-connectivity of each ROIs and the colors of the edges show the strength of connectivity.

Table III: Identified hub MNI coordination

ROI index	MNI Coordinate
FAG	(-36, -9, 39) * \triangle
FAD	(63, 6, 30) \triangle (63, 3, 33) *
F1D	(21, 60, 12) \triangle (15, 54, 15) *
F2G	(-30, 51, 30) \triangle (-33, 18, 54) * \triangle (-33, 15, 57) * (-36, 3, 60) * \triangle
F3OG	(-27, 24, -15) \triangle (-42, 42, -12) * \triangle (-51, 36, -9) *
CIAG	(-6, 15, 21) * \triangle
CIAD	(6, 15, 21) * \triangle
PQG	(-21, -48, 9) * \triangle
NCD	(6, 15, 6) * (9, 9, 15) \triangle
T3G	(-42, -33, -15) * \triangle
T3D	(51, 0, -36) \triangle (54, -33, -18) *
CERCRU1G	(-21, -87, -21) *

* and \triangle denotes the hub points appear in the case's and control's networks, respectively.

parts of a specific ROI may have interactions in different modules. Hence this voxel division gives us more detailed interaction information as well as allowing the exploration of sub-functional areas of the ROIs. Whereas the network for the control group was divided into four modules, the modular structure for the cases is more scattered and has smaller size. As we can see, for healthy individuals, the connectivity in each module is nearly symmetric (Figure 6 left column) and each module has its own rich club (Figure 6

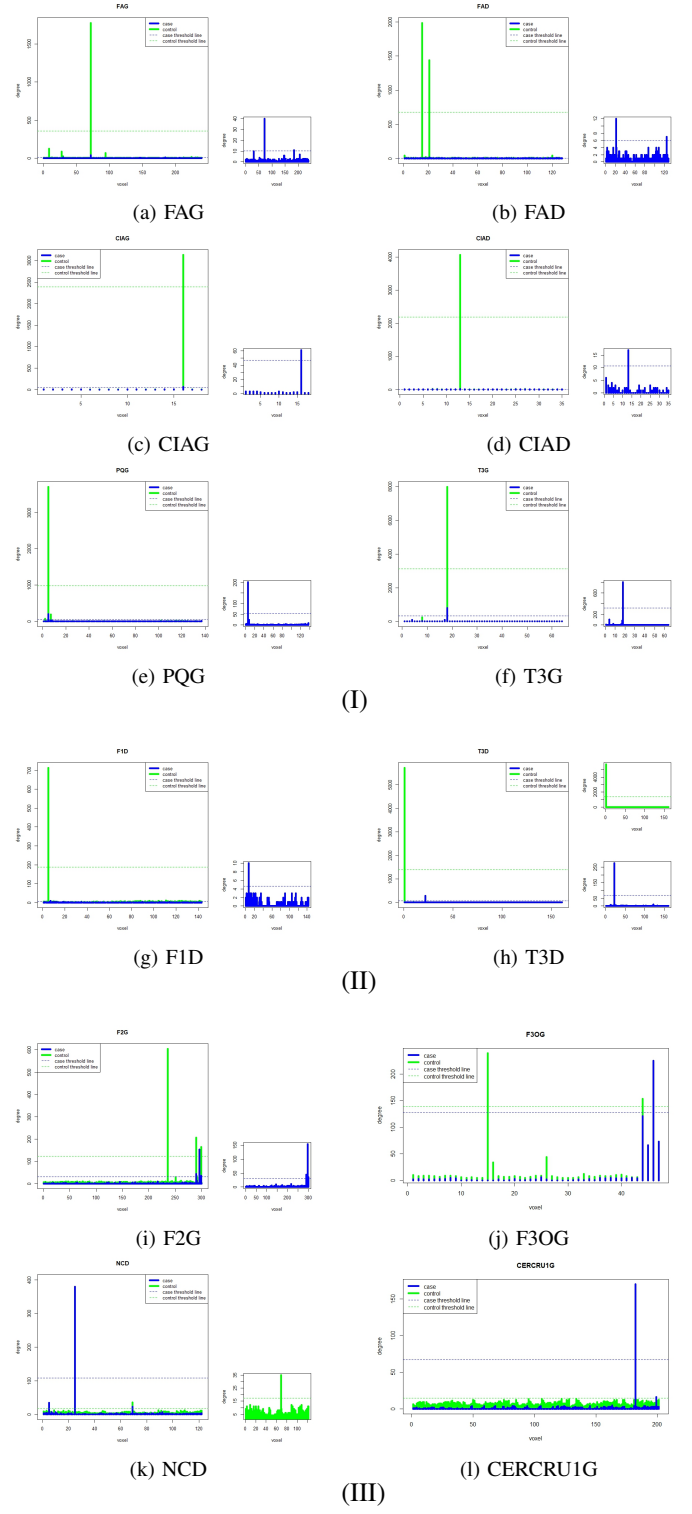


Figure 5: Connectivity performances of the voxels in selected ROIs. The x-axis is the voxel sequence and the y-axis is the degree. The threshold line is $y = \text{mean} + 3\text{sd}$, for each case respectively.

right column). We can see in the first module, although the hubs are all connected, the inferior temporal gyrus (T3) is the center with which all have strong interactions. The second module is clustered around right cingulate gyrus, anterior part (CIAD) and left hippocampus (HIPPOG). The hubs of the third module are mainly located on the frontal lobe. The last module involves the left cingulate gyrus, anterior part (CIAG), right supermarginal gyrus (GSMD), and left superior temporal gyrus (T1G). For the modular structure of SZ patients, 6 modules are exhibited in Figure 7. However, the strength of the connectivity in the case group is sharply reduced and we are unable to find any significant rich club organizations for SZ patients. In fact, in each module we only detected one central hub region which are right parahippocampus (PHIPPOD), left inferior temporal gyrus (T3G), left middle frontal gyrus (F2G), right caudate nucleus (NCD), left precuneus (PQG) and right inferior temporal gyrus (T3D), respectively.

E. Pairwise Comparison

We further applied a pairwise hypothesis test between the case and control groups for a solid statistical comparison. We followed the steps mentioned in Section 2.3, setting the significance level $\alpha_3 = 0.01$. Finally, we identified 8310 significant aberrant edges (see Figure 8). The most significant aberrant hubs are given in Table IV. Other than the aberrant hub, we were also able to find aberrant connectivity among different ROIs. In Table V, we listed the 10 pairs of ROIs that have the most abnormal connectivity strength represented by the sum of aberrant edges between the two ROIs. We further examined the connectivity within the 10 pairs of ROIs and found out the abnormal connectivity occurred in some specific sub-regions of each ROI, which are densely connected.

The location of these sub-regions are shown in Figure 9. In fact, our result also suggests the aberrant hub tends to appear at a specific area inside the ROI instead of spreading throughout the whole region and these sub-areas appear around the same locations. The affected areas are visualized using *xjView* toolbox (<http://www.alivelearn.net/xjview>).

Table IV: Identified aberrant hubs

	ROI index	degree
1	T3G 89	2396
2	FAD 2	1364
3	T3D 90	1198
4	PAD 58	653
5	CIAG 31	656
6	LINNG 47	597
7	P2G 61	551
8	F2G 7	502

IV. CONCLUSION AND DISCUSSION

During the auditory stimulation task, schizophrenia patients exhibited significantly reduced brain connectivity. Global measurements establish that SZ patients brain network patterns are less clustered with a less extensive functional integration ability than healthy people. Although the SZ brain network still keeps some of the modular structure, the rich club organization of each module is severely diminished. The most reduced

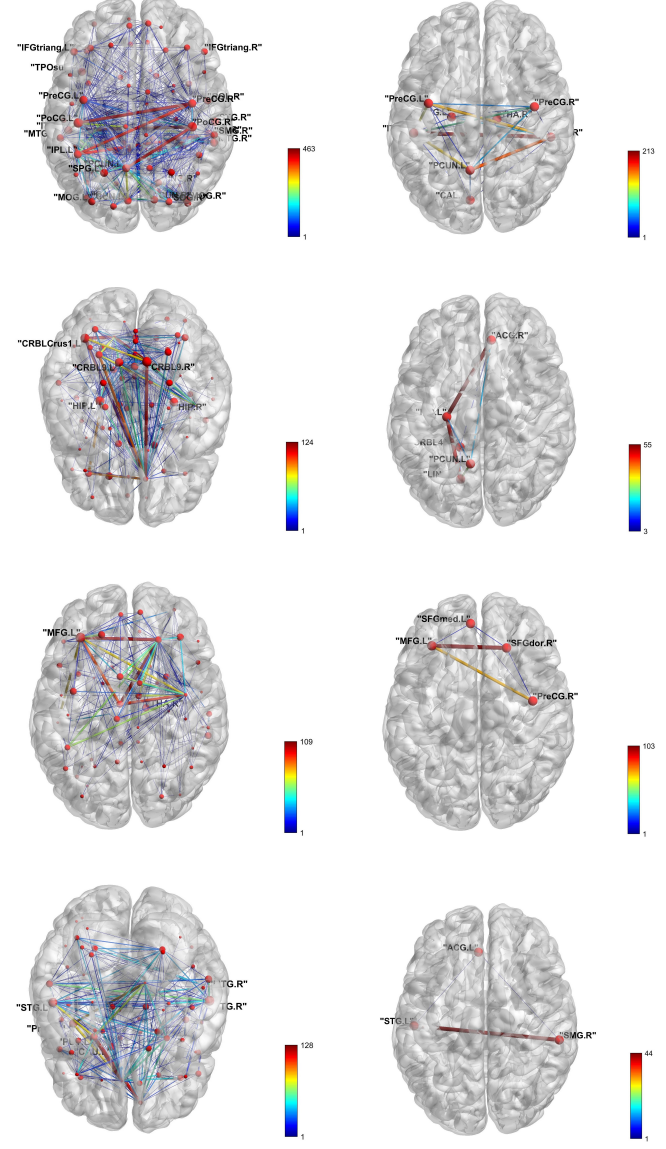


Figure 6: Axial view of the four modular patterns (left) of the brain network for healthy people and their corresponding rich club organizations (right).

Table V: Top 10 aberrant connectivity in the brain network

	ROI index	ROI index	Strength
1	FAD 2	PAD 58	320
2	PAD 58	T3G 89	224
3	P2G 61	T3D 90	185
4	F2G 7	T3G 89	184
5	PAG 57	T3G 89	156
6	P2G 61	T3G 89	154
7	F2G 7	LINGG 47	132
8	O1G 50	T3G 89	128
9	FAD 2	P2G 61	125
10	FAD 2	PAG 57	120

connectivity centers appear in the left inferior temporal gyrus (T3G), right precentral gyrus (FAD), right inferior temporal gyrus (T3D), left anterior cingulate gyrus (CIAG), left lingual gyrus (LINGG) and right anterior cingulate gyrus (CIAD).

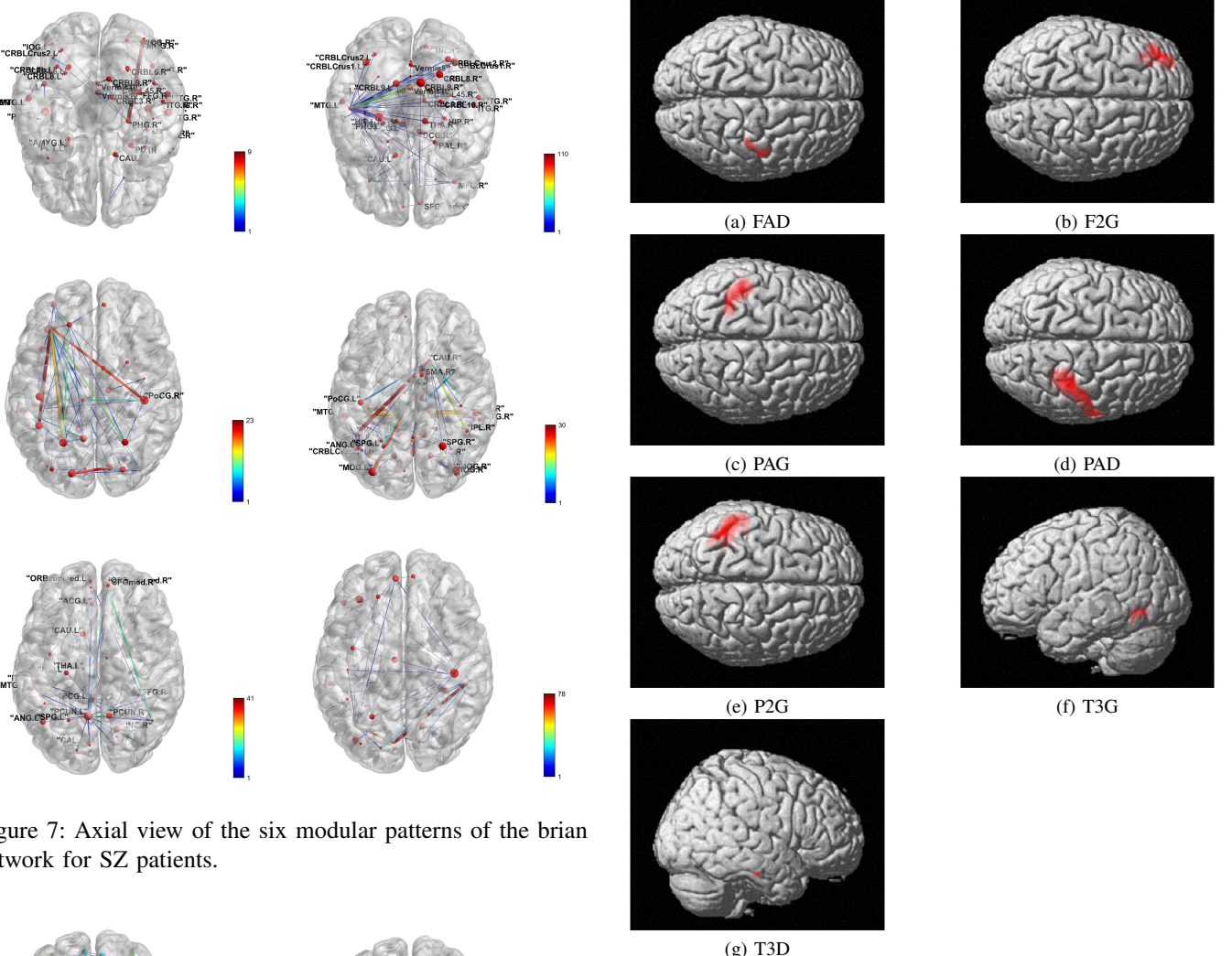


Figure 7: Axial view of the six modular patterns of the brain network for SZ patients.

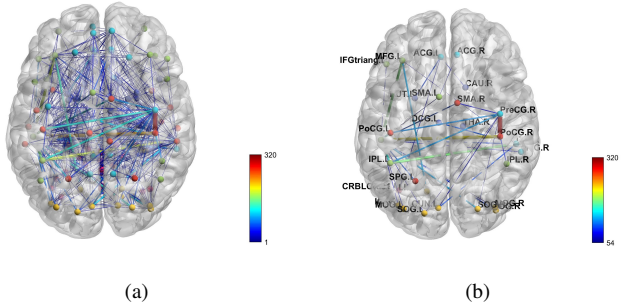


Figure 8: Visualizations of identified aberrant brain connectivities and affected hub points. Figure (a) shows the axial view of the brain. Figure (b) shows filtered edges with sparsity = 0.005.

We also observed several newly generated hub centers in right inferior temporal gyrus (T3D), right precentral gyrus (FAD) and right caudate nucleus (NCD). The most abnormal connectivity between ROIs, the region T3G and FAD appear multiple times, with the most substantial differences including FAD, PAD and T3G. Furthermore, we discovered that the abnormal connectivity is not happening region-wide, instead there exist sub-areas in each ROI where the changes occur. In all, FAD and T3G are the two brain regions that are most affected by the disease. We additionally discovered some sub-

aberrant areas which could only be achieved at voxel level. We identified some specific aberrant clustering areas within the ROIs some of which appear repeatedly. This suggests that these areas may be essential to SZ. The brain regions we identified here may be of particular interest for further neurobiological study of SZ.

Several conclusions of our study are supported by previous works. Generally, studies have found disrupted functional integration of widespread brain areas, including a decreased connectivity among the insula, temporal lobe, and prefrontal cortex [23]. Other analyses of anatomical covariance networks point to a less prominent role of high degree hub regions in the prefrontal and parietal cortex of patients [1]. Specifically, the cingulate gyrus has high influence in linking behavioral outcomes to motivation. The anterior cingulate gyrus was found to be smaller in individuals with schizophrenia [24] and the volume of grey matter was lower [25]. The inferior temporal gyrus (T3G/T3D), one of the higher levels of the ventral stream of visual processing associated with the representation of complex object features, has been shown to be related to schizophrenia [26], [27]. However, the significance

Figure 9: The affected sub-areas of each aberrant ROIs

of the precentral gyrus in SZ has not yet been well understood. As for the topology pattern, consistent with previous findings [28], [29], [30], some nodes in frontal (FAD, F2G, F3OG), parietal (PAD) areas were significantly altered in SZ. The altered topology in caudate nucleus (NCD) still needs to be verified in future research. It can be seen that there is some asymmetric performance of the brain for schizophrenia patients (see Figure 4,7) in the inferior temporal gyrus (T3), anterior cingulate gyrus (CIA), parahippocampus(PHIPPO)) caudate nucleus (NC). Actually, it has already been found that SZ patients have left-right volume asymmetries of the temporal lobe. In 1992, Shenton showed the asymmetries in the anterior hippocampus and parahippocampal gyrus [31], which play important roles in the consolidation of information from short-term memory to long-term memory and memory encoding. It is found that the patients with schizophrenia exhibit bilateral reductions in the inferior temporal gyrus [26]. Other than the temporal lobe, the caudate nucleus has shown markedly abnormal hemispheric specialization in SZ [32]. In terms of functional connectivity, decreased hemispheric connectivity and decreased intra- and inter- hemisphere asymmetry have been detected recently [33]. In addition, lateral asymmetries in cingulate gurus, inferior temporal gyrus and parahippocampus have been identified during a auditory oddball task for schizophrina patients [34]. All of these findings suggest asymmetric dysfunction in SZ and further demonstrate the biological significance and implications of our results.

The computational speed of ψ -learning method outperforms other algorithms. On a 2.8 GHz computer, ψ -learning takes 2hrs 15mins, while gLasso takes more than 7 days which was run in the package *huge* under its default setting with the regularization parameter being determined using the stability approach. However, it is still an open issue to find the optimal threshold parameter. In the future, we intend to implement the aSPU test proposed by Pan [35] for detecting group differences, which could avoid the threshold selection problem.

V. ACKNOWLEDGMENT

The work has been funded by NIH (R01GM109068, R01MH104680, R01MH107354, P20GM103472, 2R01EB005846, 1R01EB006841), and NSF (#1539067).

REFERENCES

- [1] M.P. van den Heuvel and A. Fornito, "Brain networks in schizophrenia," *Neuropsychol Rev*, vol. 24, pp. 32–48, 2014.
- [2] N. Meinshausen and P. Bühlmann, "High-dimensional graphs and variable selection with the lasso," *Annals of Statistics*, vol. 34, pp. 1436–1462, 2006.
- [3] M. Yuan and Y. Lin, "Model selection and estimation in the gaussian graphical model," *Biometrika*, vol. 94, pp. 19–35, 2007.
- [4] J. Friedman, T. Hastie, and R. Tibshirani, "Sparse inverse covariance estimation with the graphical lasso," *Biostatistics*, vol. 9, pp. 432–441, 2008.
- [5] F. Liang, Q. Song, and P. Qiu, "An equivalent measure of partial correlation coefficients for high dimensional gaussian graphical models," *J. Amer. Statist. Assoc.*, vol. 110, pp. 1248–1265, 2015.
- [6] S. Achard, R. Salvador, B. Whitcher, J. Suckling, and E. Bullmore, "A resilient, lowfrequency, small-world human brain functional network with highly connected association cortical hubs," *J. Neurosci*, vol. 26(1), pp. 63–72, 2006.
- [7] G. Gong, Y. He, L. Concha, C. Lebel, D.W. Gross, A.C. Evans, and C. Beaulieu, "Mapping anatomical connectivity patterns of human cerebral cortex using in vivo diffusion tensor imaging tractography," *Cereb. Cortex* 19 (3), pp. 524–536, 2009.
- [8] R.L. Buckner, J. Sepulcre, T. Talukdar, F.M. Krienen, H. Liu, T. Hedden, J.R Andrews-Hanna, R.A. Sperling, and K.A. Johnson, "Cortical hubs revealed by intrinsic functional connectivity: mapping, assessment of stability, and relation to alzheimer's disease," *J. Neurosci*, vol. 29 (6), pp. 1860–1873, 2009.
- [9] M.P. van den Heuvel, C.J. Stam, M. Boersma, and H.E. Hulshoff Pol, "Small-world and scale-free organization of voxel-based resting-state functional connectivity in the human brain," *NeuroImage*, vol. 43 (3), pp. 528–539, 2008.
- [10] S. Hayasaka and P. Laurienti, "Comparison of characteristics between region-and voxel-based network analyses in resting-state fmri data," *NeuroImage*, vol. 50, pp. 499–508, 2010.
- [11] Q. Yu, Y. Du, J. Chen, H. He, J. Sui, G. Pearlson, and V. D. Calhoun, "Comparing brain graphs in which nodes are rois or ica components: a simulation study," *Human Brain Mapping*, 2017.
- [12] Q. Yu, E. B. Erhardt, J. Sui, Y. Du, H. He, D. Hjelm, M. S. Cetin, S. Rachakonda, R. L. Miller, G. Pearlson, and V. D. Calhoun, "Assessing dynamic brain graphs of time-varying connectivity in fmri data: application to healthy controls and patients with schizophrenia," *Neuroimage*, vol. 107, pp. 345–355, 2015.
- [13] M. Rubinov and O. Sporns, "Complex network measures of brain connectivity: uses and interpretations," *NeuroImage*, vol. 52, pp. 1059–1069, 2010.
- [14] M. E. J. Newman, "Modularity and community structure in networks," *Proceedings of the National Academy of Sciences*, vol. 103, pp. 8577–8582, 2006.
- [15] A. P. Dempster, "Covariance selection," *Biometrics*, vol. 28, pp. 157–175, 1972.
- [16] S. Lauritzen, *Graphical Models*, Oxford: Oxford University Press, 1996.
- [17] F. Liang and J. Zhang, "Estimating the false discovery rate using the stochastic approximation algorithm," *Biometrika*, vol. 95(4), pp. 961–977, 2008.
- [18] Albert-László Barabási and Réka Albert, "Emergence of scaling in random networks," *Science*, vol. 286, pp. 509–512, 1999.
- [19] A. Fornito, A. Zalesky, and E. Bullmore, *Fundamentals of Brain Network Analysis*, Academic Press, 2016.
- [20] M. D. Humphries and K. Gurney, "Network small-world-ness: A quantitative method for determining canonical network equivalence," *PLOS ONE*, vol. 3, pp. 1–10, 2008.
- [21] D. Lin, V. D. Calhoun, and Y.-P. Wang, "Correspondence between fmri and snp data by group sparse canonical correlation analysis.,," *Medical image analysis*, vol. 18(6), pp. 891–902, 2014.
- [22] M. Xia, J. Wang, and Y. He, "Brainnet viewer: A network visualization tool for human brain connectomics," *PLoS ONE*, vol. 8(7), pp. 1–15, 2013.
- [23] Liang M., Zhou Y., Jiang T., Liu Z., Tian L., Liu H., and Hao Y., "Widespread functional disconnectivity in schizophrenia with resting-state functional magnetic resonance imaging," *Neuroreport*, vol. 17, pp. 209213, 2006.
- [24] Hironobu Fujiwara, Kazuyuki Hirao, Chihiro Namiki, Makiko Yamada, Mitsuaki Shimizu, Hidenao Fukuyama, Takuji Hayashi, and Toshiya Mura, "Anterior cingulate pathology and social cognition in schizophrenia: A study of gray matter, white matter and sulcal morphometry," *NeuroImage*, vol. 36, pp. 1236 – 1245, 2007.
- [25] G. Costain, A. Ho, D. J. Crawley, A. Pandi Mikulis, L. M. Brzustowicz, E. W. C. Chow, and A. S. Bassett, "Reduced gray matter in the anterior cingulate gyrus in familial schizophrenia: A preliminary report. schizophrenia research," *Schizophrenia Research*, vol. 122(1-3), pp. 8184, 2010.
- [26] T. Onitsuka, M. E. Shenton, D. F. Salisbury, C. C. Dickey, K. Kasai, S. K. Toner, , and R. W. McCarley, "Middle and inferior temporal gyrus gray matter volume abnormalities in chronic schizophrenia: An mri study," *The American Journal of Psychiatry*, vol. 161(9), pp. 1603–1611, 2004.
- [27] T. Takahashi, M. Suzuki, S.-Y. Zhou, R. Tanino, H. Hagino, L. Niu, Y. Kawasaki, H. Seto, and M. Kurachi, "Temporal lobe gray matter in schizophrenia spectrum: A volumetric {MRI} study of the fusiform gyrus, parahippocampal gyrus, and middle and inferior temporal gyri," *Schizophrenia Research*, vol. 87, pp. 116 – 126, 2006.
- [28] M.-E. Lynall, D. S. Bassett, R. Kerwin, P. J. McKenna, M. Kitzbichler, U. Müller, and E. Bullmore, "Functional connectivity and brain networks in schizophrenia," *The Journal of Neuroscience: The Official Journal of the Society for Neuroscience*, vol. 30(28), pp. 94779487, 2010.

- [29] Y. Liu, M. Liang, Y. Zhou, Y. He, Y. Hao, M. Song, C. Yu, H. Liu, Z. Liu, and T. Jiang, "Disrupted small-world networks in schizophrenia," *Brain*, vol. 131, pp. 945, 2008.
- [30] Q. Yu, J. Sui, S. Rachakonda, H. He, W. Gruner, G. Pearlson, K. A. Kiehl, and V. D. Calhoun, "Altered topological properties of functional network connectivity in schizophrenia during resting state: A small-world brain network study," *PLOS ONE*, vol. 6, pp. 1, 2011.
- [31] M. E. Shenton, R. Kikinis, F. A. Jolesz, S. D. Pollak, Marjorie LeMay, C. G. Wible, ..., and R. McCarley, "Left temporal lobe abnormalities in schizophrenia and thought disorder: a quantitative mri study," *New England Journal of Medicine*, vol. 327, pp. 604–612, 1992.
- [32] S. Mueller, D. Wang, R. Pan, D. J. Holt, and H. Liu, "Abnormalities in hemispheric specialization of caudate nucleus connectivity in schizophrenia," *JAMA Psychiatry*, vol. 72(6), pp. 552–560, 2015.
- [33] O. Agcaoglu, R. Miller, E. Damaraju, B. Rashid, J. Bustillo, M. Cetin, T. Van Erp, S. McEwen, A. Preda, J. Ford, K. Lim, D. S. Manoach, D. Mathalon, S. Potkin, and V. D. Calhoun, "Decreased hemispheric connectivity and decreased intra- and inter-hemisphere asymmetry of resting state functional network connectivity in schizophrenia," *Brain Imaging and Behavior*, in press.
- [34] N. Swanson, T. Eichele, G. D. Pearlson, K. A. Kiehl, and V. D. Calhoun, "Lateral differences in the default mode network in healthy controls and schizophrenia patients," *Hum Brain Mapp*, vol. 32, pp. 654–664, 2011.
- [35] Kim J, Wozniak JR, Mueller BA, Shen X, and Pan W, "Comparison of statistical tests for group differences in brain functional networks," *NeuroImage*, vol. 101, pp. 681–694, 2014.

Table VI: The Index, Abbreviation and Name of the ROIs using AAL 116

Index	Abbreviation	Name	Index	Abbreviation	Name
1,2	FA G/D	Precentral Gyrus	63,64	GSM G/D	Supramarginal gyrus
3,4	F1 G/D	Superior frontal gyrus	65,66	GA G/D	Angular gyrus
5,6	F1O G/D	Superior frontal gyrus, orbital	67,68	PQ G/D	Precuneus
7,8	F2 G/D	Middle frontal gyrus	69,70	LPC G/D	Paracentral lobule
9,10	F2O G/D	Middle frontal gyrus, orbital	71,72	NC G/D	Caudate nucleus
11,12	F3OP G/D	Inferior frontal gyrus, opercular	73,74	NL G/D	Putamen
13,14	F3T G/D	Inferior frontal gyrus, triangular	75,76	PALL G/D	Pallidum
15,16	F3O G/D	Inferior frontal gyrus, orbital	77,78	THA G/D	Thalamus
17,18	OR G/D	Rolandic operculum	79,80	HESCHL G/D	Heschl gyrus
19,20	SMA G/D	Supplementary motor area	81,82	T1 G/D	Superior temporal gyrus
21,22	COB G/D	Olfactory cortex	83,84	T1A G/D	Temporal pole superior temporal
23,24	FM G/D	Superior frontal gyrus, medial	85,86	T2 G/D	Middle temporal gyrus
25,26	FMO G/D	Superior frontal gyrus, medial orbital	87,88	T2A G/D	Temporal pole: middle temporal
27,28	GR G/D	Gyrus rectus	89,90	T3 G/D	Inferior temporal gyrus
29,30	IN G/D	Insula	91,92	CERCRU1 G/D	Cerebellum crus 1
31,32	CIA G/D	Cingulate gyrus, anterior part	93,94	CERCRU2 G/D	Cerebellum crus 2
33,34	CINM G/D	Cingulate gyrus, mid part	95,96	CER3 G/D	Cerebellum 3
35,36	CIP G/D	Cingulate gyurs, posterior part	97,98	CER4_5 G/D	Cerebellum 4 5
37,38	HIPPO G/D	Hippocampus	99,100	CER6 G/D	Cerebellum 6
39,40	PARA_HIPPO G/D	Parahippocampus	101,102	CERE7 G/D	Cerebellum 7
41,42	AMYGD G/D	Amygdala	103,104	CER8 G/D	Cerebellum 8
43,44	V1 G/D	Calcarine fissure	105,106	CER9 G/D	Cerebellum 9
45,46	Q G/D	Cuneus	107,108	CER10 G/D	Cerebellum 10
47,48	LING G/D	Lingual gyrus	109	VER1_2	Vermis 1 2
49,50	O1 G/D	Superior occipital lobe	110	VER3	Vermis 3
51,52	O2 G/D	Middle occipital lobe	111	VER4_5	Vermis 4 5
53,54	O3 G/D	Inferior occipital lobe	112	VER6	Vermis 6
55,56	FUSI G/D	Fusiform gyrus	113	VER7	Vermis 7
57,58	PA G/D	Postcentral gyrus	114	VER8	Vermis 8
59,60	P1 G/D	Superior parietal gyrus	115	VER9	Vermis 9
61,62	P2 G/D	Inferior parietal gyrus	116	VER10	Vermis 10